

THE OFFICIAL MAGAZINE OF THE OCEANOGRAPHY SOCIETY

# Oceanography

## CITATION

Magalhães, J.M., and J.C.B. da Silva. 2017. Internal waves along the Malvinas Current: Evidence of transcritical generation in satellite imagery. *Oceanography* 30(3):110–119, <https://doi.org/10.5670/oceanog.2017.319>.

## DOI

<https://doi.org/10.5670/oceanog.2017.319>

## COPYRIGHT

This article has been published in *Oceanography*, Volume 30, Number 3, a quarterly journal of The Oceanography Society. Copyright 2017 by The Oceanography Society. All rights reserved.

## USAGE

Permission is granted to copy this article for use in teaching and research. Republication, systematic reproduction, or collective redistribution of any portion of this article by photocopy machine, reposting, or other means is permitted only with the approval of The Oceanography Society. Send all correspondence to: [info@tos.org](mailto:info@tos.org) or The Oceanography Society, PO Box 1931, Rockville, MD 20849-1931, USA.

# Internal Waves Along the Malvinas Current

EVIDENCE OF TRANSCRITICAL GENERATION IN SATELLITE IMAGERY

By Jorge M. Magalhães and José C.B. da Silva

“ High-spatial-resolution multispectral satellite imagery from Sentinel-2A acquired along the Patagonian shelf and continental slope in the Southwest Atlantic Ocean has revealed intense surface manifestations of ISW-like packets propagating upstream of the Malvinas Current. ”

**ABSTRACT.** An extended satellite image data set is used to investigate the two-dimensional structure of internal waves (IWs) that propagate along the Patagonian shelf break and continental slope in the opposite direction of the Malvinas Current (MC). Intense surface manifestations of IWs are found throughout the semidiurnal and fortnightly tidal cycles, propagating more than 1,000 km in the along-slope direction between 38°S and 48°S. An instantaneous 800 km view provided by the Sentinel-2A satellite multispectral imager shows a nearly continuous IW field in which interpacket distances do not fit the usual semidiurnal tidal scales observed in coastal waters. Instead, acoustic Doppler current profiler-measured currents and CTD station data are consistent with resonant generation mechanisms in which the MC flows over bottom topography and generates upstream-propagating waves in a transcritical regime. These conditions are known to cause extra dissipation and mixing, whose effects over time and along more than 1,000 km may be important to a wider scope of ocean applications.

## INTRODUCTION

A significant amount of ocean internal wave (IW) research is motivated by understanding the processes involved in tidally driven generation, propagation, and dissipation mechanisms. Some of these studies rely on sophisticated global ocean models aimed at accurate predictions and interpretations of ocean dynamics, such as diapycnal mixing and the meridional overturning circulation (e.g., see Trossman et al., 2016). The energy budgets in these models need to account for energy transfers from barotropic tides to IW motions as they propagate over irregular bottom topography (see Buijsman et al., 2016, and references therein).

However, tidally driven processes include just a few of the mechanisms from which IWs may be generated (see Jackson et al., 2012, for a review concerning IW generation), and energy

sinks owing to IWs may be underestimated by semidiurnal frequencies alone (e.g., see Nikurashin and Ferrari, 2011). For instance, current systems in the ocean are now acknowledged as independent IW generation sources that significantly influence both deep- (Bell, 1975; Nikurashin and Ferrari, 2010) and shallow-water (e.g., Kodaira et al., 2014) IW dynamics. In this study we are particularly interested in shallow and intermediate waters, where steady currents are now known to be consistent with interfacial IW resonant generation along the ocean's pycnocline, as recently shown for the North Brazilian Current and an IW hotspot running along the Amazon continental shelf for more than 500 km (Lentini et al., 2016).

Similar IW generation mechanisms may be operational in other regions of the world ocean, especially in the presence of

steady currents whose magnitudes may be close to those predicted for linear IW phase speeds. In this case, hydraulic theories predict that resonance conditions for interfacial IWs are likely to occur. These are typically estimated using a densimetric Froude ( $Fr$ ) number that compares some measure of the average flow with the linear IW phase speed (e.g., see Melville and Helfrich, 1987, and Farmer and Armi, 1999). In fact, rank-ordered packets of internal solitary waves (ISWs; i.e., single-crested, near-permanent wave forms identified with weakly nonlinear wave solutions) are widely documented in the ocean and are generated whenever  $Fr \approx 1$  (e.g., see da Silva and Helfrich, 2008, and references therein). This is expected to be particularly important in quasi-steady currents, because the time scales involved should allow isopycnal disturbances to grow in time as energy is drawn from the mean flow—which means that wave packets will form continuously as long as the forcing persists (Redekopp and You, 1995).

High-spatial-resolution multispectral satellite imagery from Sentinel-2A acquired along the Patagonian shelf and continental slope in the Southwest Atlantic Ocean (see Figure 1 for location) has revealed intense surface manifestations of ISW-like packets propagating upstream of the Malvinas Current (MC), similar to those found along the Amazon shelf (see Lentini et al., 2016).

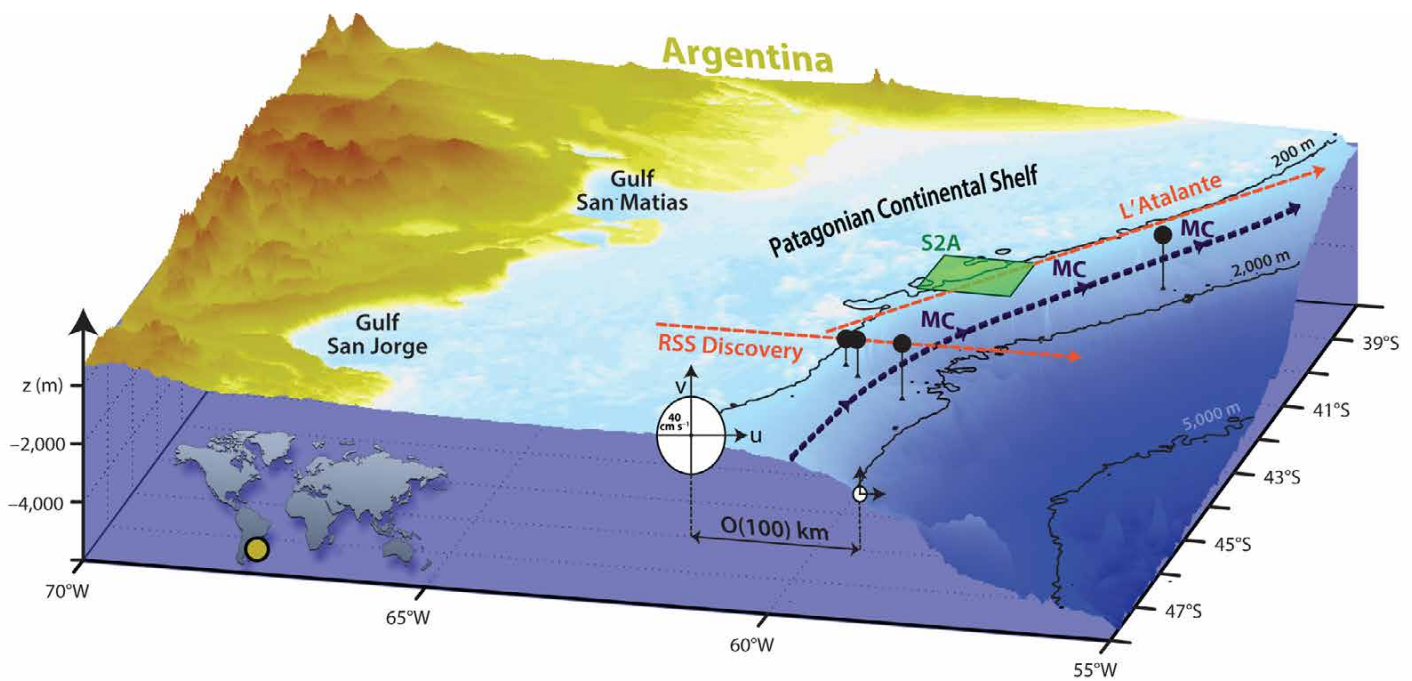


**FIGURE 1.** Continental margin in the southwest Atlantic Ocean between 38°S and 48°S (see inset in bottom left corner). Selected isobaths are shown as solid black lines together with representative tidal ellipses for depths of 200 m and 2,000 m. A dashed black line between them depicts the mean Malvinas Current (MC). Two red lines highlight acoustic Doppler current profiler (ADCP) sections used in this study, with corresponding CTD stations indicated by solid black circles. The green shaded area marks the Sentinel-2A (S2A) acquisition in Figure 2a.

Previous observations in this study region also documented ISW-like packets propagating in the cross-shelf direction north of 35°S (Jackson, 2004). Jackson (2007) presents additional evidence using Moderate Resolution Imaging Spectroradiometer (MODIS) imagery that reveals waves propagating off the Patagonian continental shelf.

However, this extensively studied region (see a review in Mugetti et al., 2004) has not yet been fully investigated for the presence of IWs and their two-dimensional horizontal structure. It is possible that the MC current influences the resonant generation of IWs, whose resuspension of sediments and mixing are especially strong in shallow and intermediate waters (Bogucki et al., 1997).

The present study is motivated by the availability of an extended satellite data set acquired between 38°S and 48°S. These images display the presence of high-frequency IWs propagating southward along the shelf break and continental slope. We document the waves' two-dimensional horizontal structure, including spatial dimensions, lifespan, and observational frequency. Together with additional in situ data, we seek a

plausible IW generation mechanism consistent with the satellite observations.

The next section discusses the relevant oceanographic background for IWs in the study region. We then describe the satellite data set and what we learned about IW dynamics. This information is then used together with available in situ data to provide the details of wave generation and propagation upstream of the MC. The last section of the paper summarizes our findings.

### STUDY REGION

Our study region is the Southwest Atlantic Ocean where continental margins stretch for several thousand kilometers and are among the largest in the world (Etcheverry et al., 2016). We are particularly interested in shallow and intermediate depths along the shelf break and continental slope between 38°S and 48°S (Figure 1). At these latitudes, bottom slopes average around 1° between 200 m and 2,000 m depth—somewhat gentle slopes that extend approximately 100 km in the cross-shelf direction (see Figure 1).

Because the MC is mainly steered along the continental slope, it carries colder Antarctic waters toward higher

latitudes until it eventually meets the opposing Brazil Current in what is commonly referred to as the Brazil/Malvinas Confluence region (Combes and Matano, 2014). A recent study using remote-sensing and in situ data revealed important details of the MC's horizontal and vertical structure that are especially important to this study (see Piola et al., 2013). In particular, two narrow jets (10–20 km wide) were found extending nearly 1,000 km along the continental slope and closely following the 200 m and 1,400 m isobaths. An acoustic Doppler current profiler (ADCP) section along 45°S (see Figure 1 for location) shows typical velocities to be of the order of 1 m s<sup>-1</sup> in both cores. Additional measurements along the MC were also obtained from a towed ADCP running approximately in the along-shelf direction (available online at <http://www.ifremer.fr>). In this case, the French research vessel *L'Atalante* steamed northeastward (see Figure 1 for location), revealing significant variability also of the order of 1 m s<sup>-1</sup> at scales between 50 km and 100 km within just a few hours (further discussed below).

Simultaneous with this steady flow is the barotropic tide, which is mainly

semidiurnal along the Patagonian shelf and continental slope. A regional tidal solution using the Oregon Tidal Inversion Software running at  $1/30^\circ$  (<http://volkov.oce.orst.edu/tides/PatS.html>; see Egbert and Erofeeva, 2002) reveals that meridional variability in tidal currents is small at scales of at least 100 km. However, tidal currents change significantly in the cross-shelf direction, with maxima that decrease rapidly from  $40 \text{ cm s}^{-1}$  to  $5 \text{ cm s}^{-1}$  between the shelf break and the 2,000 m isobath (see Figure 1). Comparable variability of the order of  $20 \text{ cm s}^{-1}$  is also found at shallow depths within a spring-neap tidal cycle, which decreases to almost zero beyond 2,000 m depth. This means that two different flows (i.e., MC and tides) are constantly interacting in the study region, resulting in strong stratified currents flowing over irregular bottom bathymetry—known conditions for significant IW activity, as shown for other coastal regions (e.g., Bogucki et al., 1997; Farmer and Armi, 1999; da Silva and Helfrich, 2008; Lentini et al., 2016).

At these latitudes, stratification conditions, which are essential for IW propagation, are expected to have considerable seasonal variability. Monthly means obtained from <http://www.esrl.noaa.gov> indicate that suitable stratification capable of sustaining IWs exists approximately between November and May, then weakens between July and September, with June and October being somewhat transition months (see online supplemental Figure S1). The observations made using satellite imagery are consistent with this seasonal variability; waves are observed year-round except during the austral winter when stratification is supposedly too weak to support IW propagation.

### SATELLITE IMAGERY ANALYSIS

A significant amount of IW research has been done over the last few decades based on unique insights provided by satellite observations. Satellite-borne synthetic aperture radars (SARs) and imaging spectrometers are particularly useful in revealing the details of otherwise unexplored

IW fields (e.g., see Jackson et al., 2012, and da Silva et al., 2015). While SARs rely on active measurements of sea surface roughness patterns induced by IWs, passive imaging spectrometers use the reflection of sunlight from the ocean surface (i.e., sunglint) to detect the waves'

surface manifestations (for more details see Alpers, 1985; da Silva et al., 2000; and Jackson, 2007; Jackson and Alpers, 2010).

Figure 2a is an example of data from the Sentinel-2A satellite sensor (a passive imaging spectrometer) collected along the Patagonian continental slope,

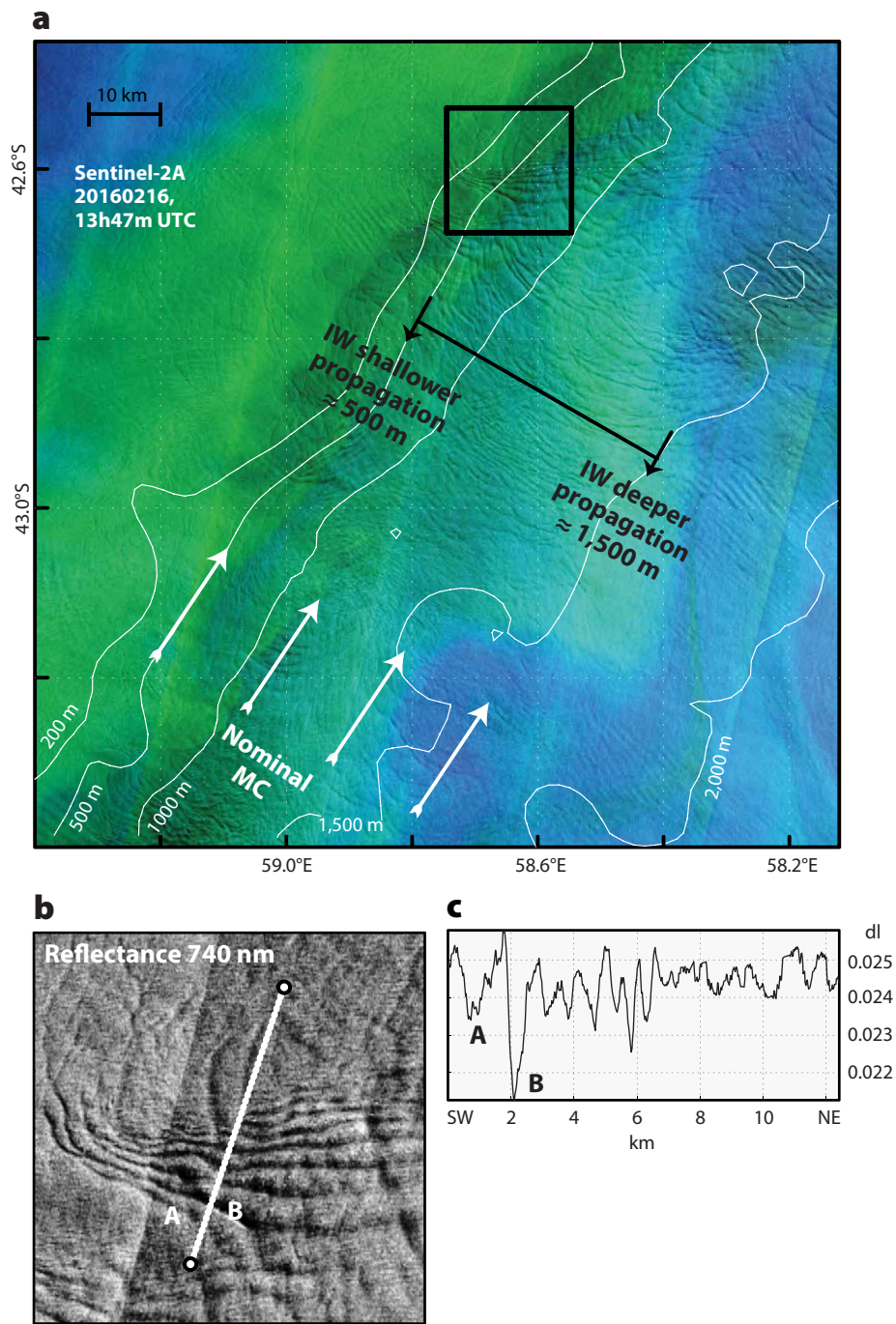


**FIGURE 2.** (a) RGB composite for a Sentinel-2A (passive imaging spectrometer) acquisition from February 16, 2016. Selected isobaths are depicted in white. Internal waves (IW) are seen propagating in a general southwest direction (black arrows) against a nominal MC (white arrows), mainly along two distinct depths (black arrows). (b) A zoom-in on the black square in (a) using reflectance in band 6 centered at 740 nm. (c) Transect corresponding to white line in (b) with the first two waves labeled A and B.

where an RGB composite reveals the two-dimensional horizontal structure of an IW field near 43°S. In this example, several ISW-like packets are found propagating southwestward (Thompson and Gasparovic, 1986), with surface patterns that appear as brighter and darker strips when compared to the unperturbed background (see also Figure 2b). These surface patterns are characteristic of sunglint surface manifestations of mode-1 rank-ordered ISW-like packets propagating along a stratified pycnocline; here, near-surface currents create convergence and divergence patterns that appear as brighter and darker strips (respectively) as a result of hydrodynamic modulation of the wind wave field. A closer inspection of Figure 2a also shows a near-continuous distribution of IWs propagating along the shelf break and continental slope, within which distinct packet structures may be identified (as highlighted in the black squared frame). Also, while the majority of the observed waves propagate southwestward along the 500 m isobath,

a second smaller set of IWs is also seen north of 42.8°S propagating approximately along the 1,500 m isobath.

Figure 2b,c shows typical horizontal packet structures, in which an image profile corresponds to a representative packet in Figure 2a. According to this example, representative dimensions of a typical wave packet are between 3 km and 10 km. In this particular case, at least eight individual waves can be identified, each with a wavelength of ~1 km (in the direction of wave propagation), which is also a representative scale for individual IWs in this region. Note also that waves in Figure 2b are observed to reach along-crest lengths between 5 km and 15 km, which may be considered a typical range for these observations.

Despite presenting several well-developed wave packets (such as the one highlighted in Figure 2b), the overall impression of Figure 2a is that of a near-continuous IW field whose inter-packet distances do not fit the typical semidiurnal scales expected for these

depths (around 40 km, assuming a depth of 500 m) when compared with other known IW hotspots (e.g., see Jackson, 2004). Interestingly, the characteristics in this 100 km × 100 km subset are representative of the entire study region. In fact, Figure 2a is part of a much larger collection of images acquired as Sentinel-2a flew approximately between 41°S and 48°S. Online supplemental Figure S2 is a mosaic that joins these images, along with selected isobaths, to provide a simultaneous view of the IW field along more than 800 km. Just as in Figure 2a, the majority of the observed waves are found propagating along the continental slope in a general southwestward direction; again, a main cluster is found approximately along the 500 m isobath, whereas a smaller set of waves is sometimes found between depths of 1,000 m and 2,000 m. The inter-packet distances are also irregular, ranging between 3 km and 20 km, which means that typical scales for mode-1 semidiurnal periods do not occur in this region (i.e., around 40 km assuming a depth of 500 m). Instead, just as in Figure 2a, the satellite imagery in this case gives the impression of a nearly continuous IW field propagating southwestward along the continental slope.

A composite view showing the locations of only the strongest wave packets identified in supplemental Figure S2 is presented in Figure 3a (green circles), confirming the high spatial density of these observations. Cloud cover limits this view above 41°S, but MODIS imagery (available at <https://worldview.earthdata.nasa.gov>) reveals that these waves reach as far north as 38°S, and hence to the edge of the Brazil/Malvinas Confluence region.

An extended data set was therefore assembled, gathering 71 satellite acquisitions that were considered representative of the study region; they were used to investigate the full two-dimensional structure of the IW field propagating along the Patagonian shelf break and continental slope. This data set includes 33 TerraSAR-X images,

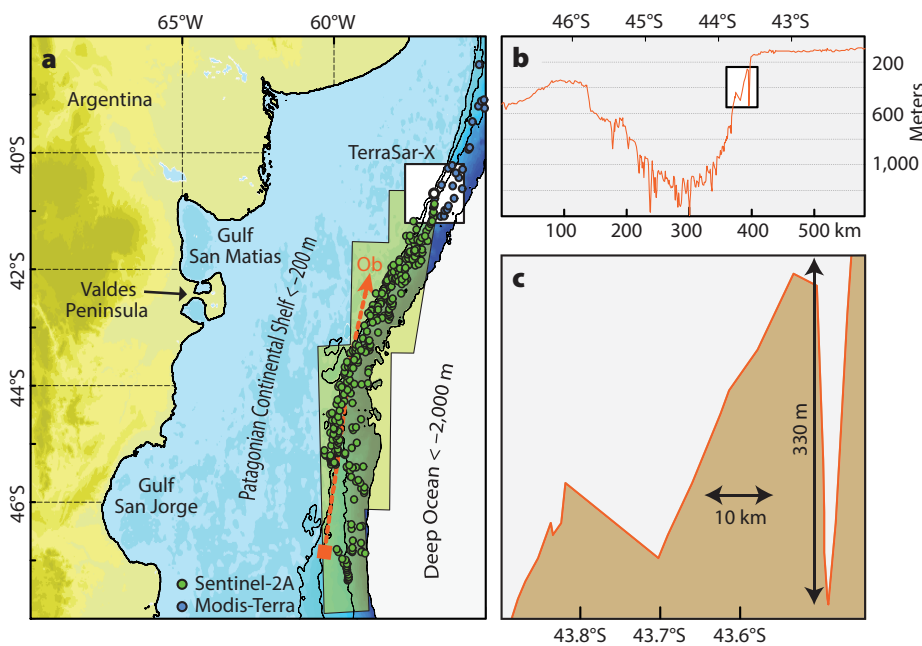


**FIGURE 3.** (a) A composite map of wave packet locations identified in Sentinel-2A acquisitions from February 16, 2016, and shown in supplemental Figure S2 (green circles), surrounded by green shading. Observations from a MODIS-Terra image acquired seven days earlier were added north of 41.5°S (blue circles). Black lines indicate 200, 500, 1,000, and 2,000 m isobaths, and the white rectangle encloses the TerraSAR images discussed in Figure 4a. The red line represents part of a high-resolution bathymetric survey. (b) Bathymetric profile along the red line in (a). (c) Zoomed-in section corresponding to white rectangle in (b).

12 Envisat-ASAR, and 1 ERS-SAR acquisitions, six long strips from Sentinel-2A, and 19 MODIS-Terra and -Aqua images. The data set spans the period from January 2000 to December 2016, with all observations collected between November and May when stable stratification allows IW propagation.

Just as in Figure 2a, the image data set consistently shows significant IW activity propagating southwestward between 38°S and 48°S. Unlike other coastal regions, however, the frequency of the observed waves appears to be tidally independent. For instance, according to Figure 4a, the 33 TerraSAR-X wave observations are found evenly scattered across the semi-diurnal and fortnightly tidal cycles. Note these images were collected within a reduced area of the study region (see Figure 3a), revealing that IWs are persistently observed there with no apparent relation to tidal currents. Nonetheless, the remaining SAR and MODIS observations of waves in Figure 4a were evenly acquired along the entire study region, and they too were spread evenly across

the tidal cycles, suggesting a persistent wave field between 38°S and 48°S.

An additional collection of MODIS images (available at <https://worldview.earthdata.nasa.gov>) confirms the strong presence of IWs in the study region. Figure 4b presents the results of an IW survey between 2014 and 2016, using January as a representative summer month, as it provides the best cloud-free and sunglint conditions between 38°S and 48°S. Note that two satellite passes covering most of the study region are available daily, approximately three hours apart from Terra and Aqua satellites. This means that the meridional extent of the continental slope along which IWs are observed can be estimated twice in any given day, as presented in Figure 4b. As expected, optimal sunglint conditions contribute to a higher distribution centered at 43°S because IW surface manifestations fade quickly outside the sun's specular reflection. Fewer IW observations were also found further north in the Brazil/Malvinas Confluence region (known to extend as far south as 40°S),

and further south owing to increased cloud coverage. Therefore, Figure 4b should be interpreted as a lower threshold for IW observations, suggesting they are frequently observed along more than 1,000 km. In fact, there was no MODIS available for only 17 of the 93 days we studied (i.e., all days in January for 2014, 2015, and 2016), and SAR images on three of the 17 days with no MODIS revealed equally intense IW activity.

### RESONANT GENERATION OF IWs

The satellite observations consistently show a nearly continuous IW field for more than 1,000 km between 38°S and 48°S along the Patagonian shelf break and continental slope. However, the wave packets are irregularly spaced rather than exhibiting typical semidiurnal wavelengths as observed in other coastal regions (e.g., Jackson, 2004; da Silva et al., 2009; Magalhães and da Silva, 2012). It is also interesting to note that numerical models show little or no semidiurnal IW energy in this region (e.g., see Figure 4 in Buijsman et al., 2016).

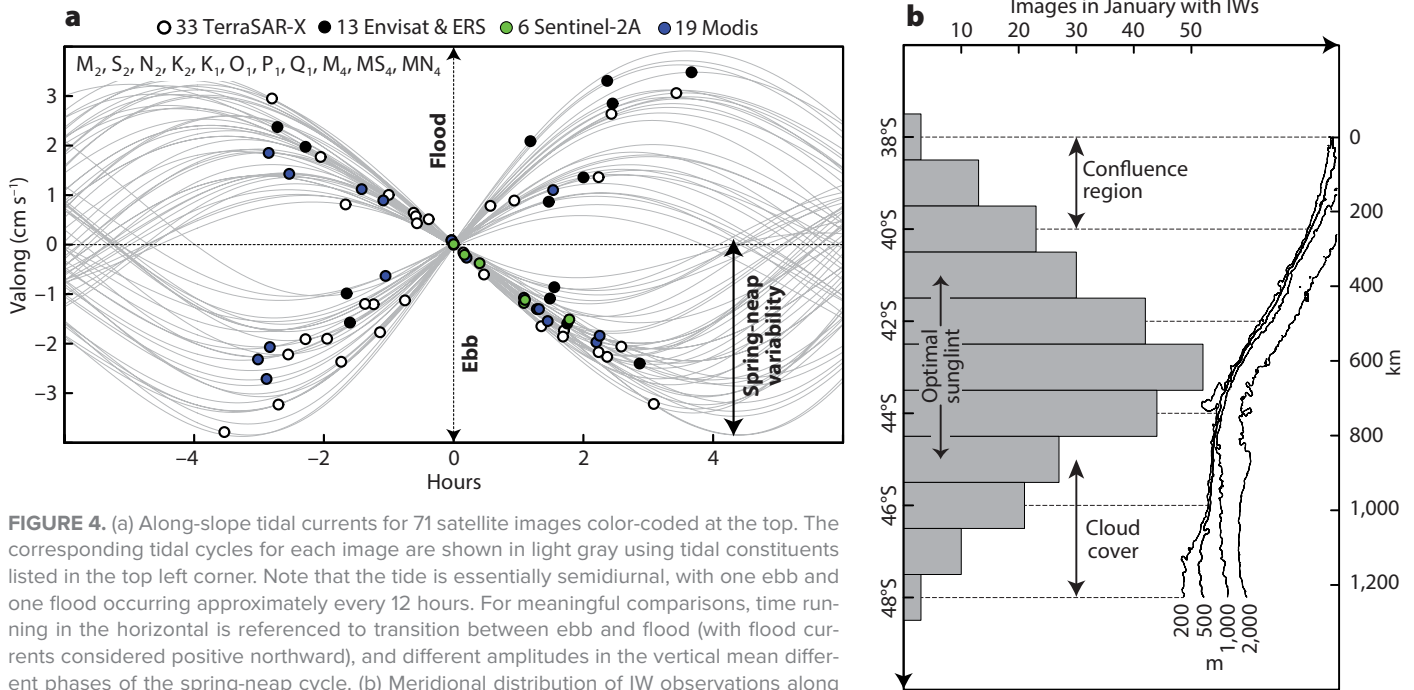


**FIGURE 4.** (a) Along-slope tidal currents for 71 satellite images color-coded at the top. The corresponding tidal cycles for each image are shown in light gray using tidal constituents listed in the top left corner. Note that the tide is essentially semidiurnal, with one ebb and one flood occurring approximately every 12 hours. For meaningful comparisons, time running in the horizontal is referenced to transition between ebb and flood (with flood currents considered positive northward), and different amplitudes in the vertical mean different phases of the spring-neap cycle. (b) Meridional distribution of IW observations along the Patagonian shelf and continental slope as observed in MODIS imagery for January between 2014 and 2016. Representative isobaths are shown for reference together with the additional scale on the right, in which distance is measured beginning from 38°S along the 500 m isobath. See text for more details.

Therefore, we seek an IW generation mechanism that is consistent with the satellite imagery, recalling that the majority of the IWs are observed as propagating upstream of the MC (see Figures 1 and 3). In this region, a stratified current flows steadily over bottom topography. Similar conditions have been shown to generate upstream-propagating IWs along the Amazon shelf, provided there is enough forcing by bottom bathymetry (Lentini et al., 2016).

A high-resolution bathymetric survey conducted from the Russian research vessel *Ob* was approximately in the along-slope direction (see Figure 3a), and hence within the waves' propagation path. The Figure 3b bathymetric profile indicates considerable seafloor roughness between 42°S and 47°S at horizontal scales between 3 km and 10 km, and therefore at length scales of the same order as the observed IW packets (see also supplemental Figure S2). Note, for instance, that the IWs observed near 43.4°S (in Figure 2a) are coincident with steep bottom topography that rises and falls more than 300 m on horizontal scales of the order of 10 km (as seen in Figure 3c). Several other surveys identified along

the Patagonian continental slope confirm similar bottom slopes directly along the MC (available at <https://maps.ngdc.noaa.gov/viewers/bathymetry>).

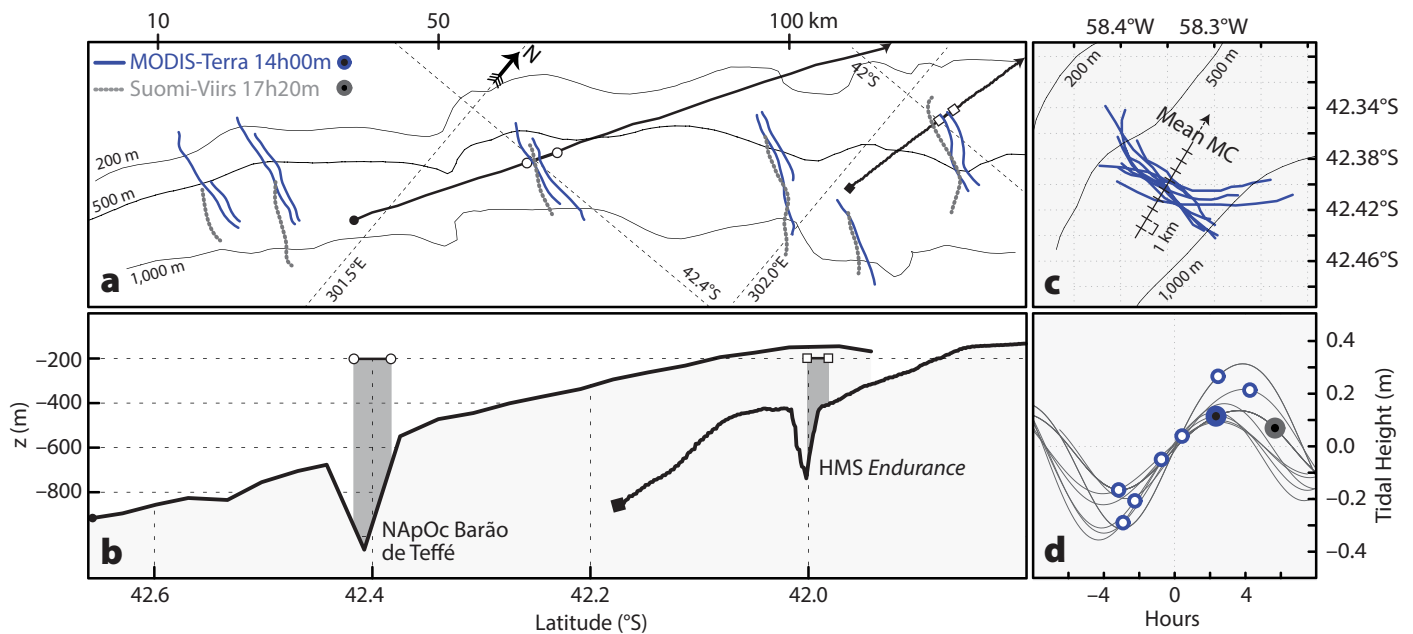
Figure 5a compares the strongest IWs observed from two satellite acquisitions approximately three hours apart (see also supplemental Figure S3). These IWs appear to be closely related to steep seafloor topography (Figure 5b), remaining arrested at these locations for at least three hours. A composite map joining similar MODIS observations (all within January 2016) suggests that this correlation is a recurring feature, as all leading IWs from similar wave packets appear clustered within fewer than 10 km (see Figure 5c). Tidal currents in this case again appear to have no influence on the observed waves, as quite distinct tidal phases have no consequence in the composite outcome (see Figure 5d).

Figure 5 is therefore consistent with some generation mechanism resulting from the interaction of the MC and the underlying seafloor topography. The forcing effect of stratified flow over bottom obstacles is usually estimated via a densimetric (or internal) Froude number ( $Fr$ ), which compares the magnitude of the

stratified flow ( $U$ ) with the corresponding linear IW phase speed ( $c$ ). In the particular case of the Patagonian shelf break and continental slope, the contribution from tides and the MC needs to be considered as follows:

$$Fr = \frac{U}{c}, U = U_{tides} + U_{MC}. \quad (1)$$

In the examples that follow,  $U_{tides}$  is computed from the regional solutions available from <http://volkov.oce.orst.edu/tides/region.html>, and  $U_{MC}$  is the depth-mean flow computed from the ADCP data. The flow is then said to be in critical ( $Fr = 1$ ), subcritical ( $Fr < 1$ ), or supercritical ( $Fr > 1$ ) regimes, depending how these two characteristic velocities compare. In practice, however, a transcritical band is often used to characterize near-critical conditions (i.e.,  $Fr \approx 1$ ), during which isopycnal disturbances accumulate energy from the mean flow through resonance and generate upstream-propagating packets of interfacial IWs. Note that strong supercritical flows force internal perturbations to propagate downstream as forcing velocities supersede those of the corresponding linear IWs, whereas strong subcritical waves continually escape



**FIGURE 5.** (a) Bathymetric map using Smith and Sandwell (1997) 1-minute bathymetry, together with a composite map depicting the strongest IWs in two acquisitions dated January 31, 2016. (b) Two single-beam high-resolution bathymetric profiles corresponding to the black arrows in (a). (c) Composite map using MODIS observations acquired in January 2016. (d) Same as Figure 4a for IWs shown in (a) and (c).

upstream of the mean flow (e.g., see Melville and Helfrich, 1987).

A Froude number analysis is presented in Figure 6 using towed ADCP measurements from R/V *L'Atalante* taken along the continental slope approximately between 40°S and 44°S (see also Figure 1). These measurements, available at <http://cersat.ifremer.fr>, were collected between November 3 and November 4, 2010, and thus are within the waves' observational period. Note that over 400 km were covered in fewer than 24 hours, during which some variability in the vertically averaged flow is seen on scales of the order of 100 km (see  $U_{MC}$  in blue shading in Figure 6a). However, averages above  $0.5 \text{ m s}^{-1}$  dominate until approximately 42°S when bottom depths exceed 1,000 m, and then drop below  $0.5 \text{ m s}^{-1}$  as the ship moves into shallower water. Note that this is in agreement with the MC horizontal structure, in which multiple jets add significant variability in the cross-shelf direction (Piola et al., 2013). Representative tidal currents in a spring-neap cycle were designated  $U_{tides} = \pm 10 \text{ cm s}^{-1}$ , which are mean values along the 1,000 m isobath. A boundary value problem was also solved in the same fashion as Smyth et al. (2011) and da Silva et al. (2015) to estimate  $c$  in Equation 1, considering a wavelength of 3 km and local stratification conditions for November (retrieved from in situ data available at <https://www.nodc.noaa.gov>; see Figure 1 for locations). We note in passing that 3 km is a representative scale for the wave packets observed in supplemental Figure S2. In the framework of resonant generation, this characteristic length is considered here as a proxy for the interfacial disturbances originating near forcing bathymetry as a result of the stratified flow. Note that the characteristic length of these interfacial disturbances usually compares with the already developed packets rather than with their individual waves (e.g., see Farmer and Armi, 1999, and Chen et al., 2017). Nonetheless, changing this length scale results in changes at most of about  $0.1 \text{ m s}^{-1}$  in  $c$

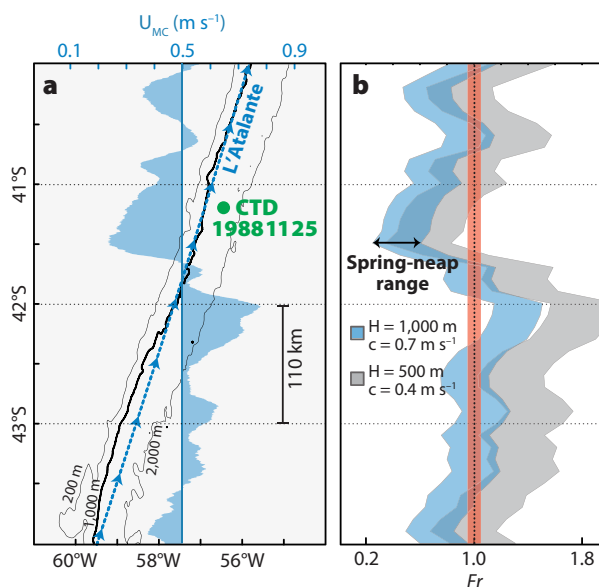
in Equation 1 (when considering a depth of 500 m, where most of the observations were made). This means the  $Fr$  estimates discussed below would remain essentially the same, with  $Fr$  variability owing mainly to changes in the mean flow (i.e.,  $U$  in Equation 1).

Figure 6b presents the overall effect of these constraints in the waves' hydraulic regime. Note that for simplicity we consider the absolute magnitude of  $Fr$ , although in this case the mean flow and the IWs propagate in opposite directions. A transcritical band is also depicted in red as  $Fr = 1 \pm 0.05$ , meaning isopycnal perturbations may remain "trapped" while draining energy from the mean flow. According to these results, plausible conditions for a transcritical regime exist approximately between 42°S and 44°S, when considering bottom depths around 1,000 m (in blue shading). Further north, the mean MC decreases substantially, consequently shifting the  $Fr$  band to subcritical conditions. Interestingly, however, decreases in the mean MC may be compensated by simply adjusting depth (and hence  $c$ ). For instance, if a shallower bottom of 500 m is considered instead, subcritical  $Fr$  values quickly shift back to the transcritical band (see gray shading in Figure 6b)—a consequence of  $c$  decreasing from 0.7–0.4  $\text{m s}^{-1}$ .

A cross-shelf  $Fr$  analysis is also presented along 45°S (see Figure 1 for

location) using the same ADCP data as in Piola et al. (2013), collected from the British RSS *Discovery* on December 28, 1992 (available at <http://www.ewoce.org/data/index.html#ADCP>). According to Figure 7a, the jet-like structure is clearly identified in the northward velocity component ( $v$ ), with increased flow seen around 300.1°E and 300.8°E. Interestingly, IW observations clustering within these jets are also identified around 45°S (seen, for example, in supplemental Figure S4 and depicted by blue rectangles in Figure 7a), and in fact along most of the study region (e.g., in Figure 2a and supplemental Figures S2 and S3).

The corresponding  $Fr$  estimates were again computed using phase speeds solved via a boundary value problem with a representative wavelength of 3 km and three CTD stations taken coincidentally with the ADCP data (shown in Figure 7b). In this case, tidal contributions were computed every  $0.1^\circ$  between 300°E and 301.1°E because they change significantly between the shelf break and the edge of the continental slope. According to Figure 7c, there is stronger spring-neap variability along the shelf break that decays rapidly in deeper waters to near-negligible tidal currents (gray envelope). If a transcritical band is again chosen as  $Fr = 1 \pm 0.05$ , a combined flow (i.e., MC and tides) results in Froude numbers oscillating with large



**FIGURE 6.** (a) ADCP section from R/V *L'Atalante* as it steamed along the Patagonian continental slope (see selected isobaths in black for reference). The top axis refers to the depth-averaged flow  $U_{MC}$  shown in blue shading (considered in the along-ship direction). (b) Froude number estimates using the CTD station in the left panel (see also Figure 7b) for depths of 500 m and 1,000 m. Envelopes account for variability in a spring-neap cycle. The  $Fr$  number range in red defines a transcritical band discussed in the text.

amplitudes around 1 within IWs Jet A. This means that while a transcritical regime is still predicted, tidal currents may shift them either to subcritical or supercritical flow. Interestingly, satellite observations showing signs of IW refraction and propagation toward the coast do appear occasionally along the shelf (see supplemental Figure S2). However, as tidal contributions fade away off-shelf,  $Fr$  variability narrows significantly and the hydraulic regime decreases largely to subcritical conditions between 300.2°E and 300.8°E. Finally, the MC contribution increases again around the 1,500 m isobath, at which point  $Fr$  values are seen to rise to the transcritical band (consistently with IWs Jet B).

The along- and cross-slope analyses from Figures 6 and 7 therefore suggest a hydraulic regime along the Patagonian shelf break and continental slope consistent with a transcritical regime, as it includes considerable periods of  $Fr = O(1)$ .  $Fr$  variability in the cross-slope direction appears to come mainly from the MC jet like-structure, whereas tidal currents in a spring-neap cycle also add

some variability but are limited close to the shelf break. The along-slope variability is mainly due to changes in the MC, because in this case changes in the tidal currents are small compared with those in the steady flow. Nonetheless, the range over which  $U_{MC}$  and  $U_{tides}$  combine is still comparable to that predicted for  $c$  in Equation 1 when considering depths between 200 m and 2,000 m, with both characteristic velocities (i.e.,  $U_{MC} + U_{tides}$  and  $c$ ) being of the order of  $1 \text{ m s}^{-1}$ . This means reasonable changes in the mean flow over shallow and intermediate depth seafloor may frequently be accommodated at some depth to still yield plausible resonant generation of IWs.

### SUMMARY AND CONCLUSIONS

An extended satellite image data set provides the first two-dimensional horizontal structure of an IW field propagating along the Patagonian shelf break and continental slope, and extending over 1,000 km between 38°S and 48°S. IWs in this region are frequently observed during spring and summer, regardless of the semidiurnal and fortnightly tidal cycles.

The majority of the observations are consistent with upstream-propagating waves in a direction opposite to the MC (Figures 1 to 3). Typical inter-packet length scales observed from satellite images appear strongly related to seafloor topography rather than to scales typical of semidiurnal tides (see Figures 2, 3, and 5), and a Froude number analysis is consistent with resonant generation mechanisms (see Figures 7 and 8).

Therefore, the present study provides evidence of a transcritical regime consistent with theories of IW resonant generation, in which the MC is likely to generate upstream-propagating IWs as it flows over the shelf break and continental slope. Tidal currents were found to be important only at the shallower depths near the shelf break, which may cause the steady flow to oscillate between subcritical and supercritical conditions (see Figure 7).

The large extension of the IW field inferred from the satellite data set presented in this paper together with the high frequency of the observations (Figures 3 and 4), make IWs potentially important along the Patagonian shelf break and continental slope, as considerable dissipation and extra mixing might be expected to occur. In particular, stratified flows in the absence of background shear exhibit their largest IW-induced shear within the top layers (Bogucki and Garrett, 1993). This, however, changes for IWs propagating upstream of a sheared flow. Note that as shear increases, the maximum IW-induced shear shifts downward toward the seafloor—a consequence of combining the wave's velocity structure with the background sheared flow. This may result in additional sediment resuspension and mixing in shallow and intermediate depths (Bogucki et al., 1997). If we are to understand the implications of these waves in vertical mixing, this particular study region is thus worthy of further research, including dedicated measurements of vertical diffusivity and numerical modeling. 

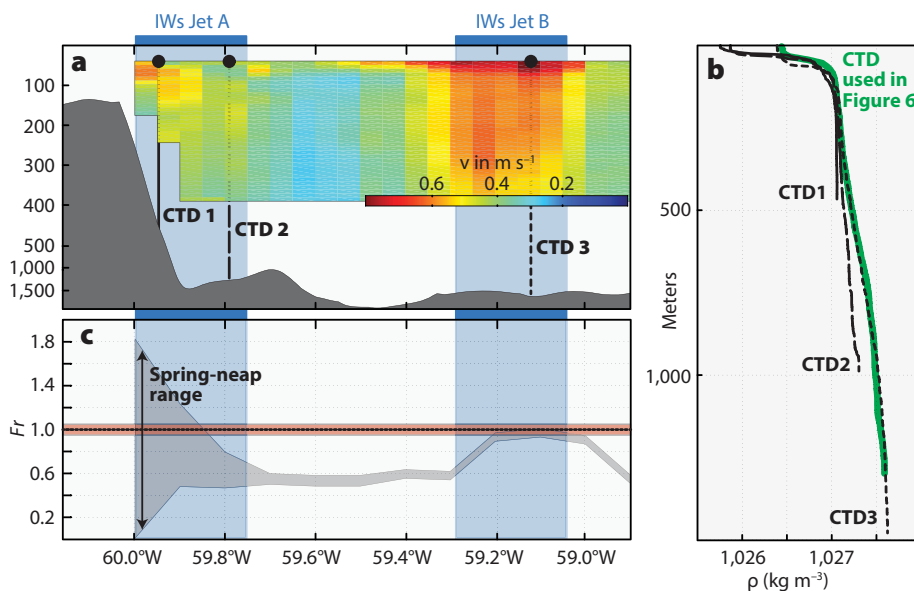


**FIGURE 7.** (a) Bathymetric section and ADCP meridional velocities (i.e.,  $v$ ) along 45°S. The approximate longitude ranges where IWs cluster in supplemental Figure S4 are depicted in blue shaded rectangles and labeled IWs Jet A and B. Three CTD stations are also marked by black circles and vertical black lines. (b) Potential density corresponding to CTDs in (a). The green line depicts the potential density for the CTD in Figure 6a. (c)  $Fr$  estimates using the CTD stations in top panel (a). The red envelope defines a transcritical band, while the gray envelope accounts for variability in a spring-neap cycle.

## SUPPLEMENTARY MATERIALS

Supplemental Figures S1–S4 are available online at <https://doi.org/10.5670/oceanog.2017.319>.

## REFERENCES

- Alpers, W. 1985. Theory of radar imaging of internal waves. *Nature* 314:245–247, <https://doi.org/10.1038/314245a0>.
- Bell, T.H. Jr. 1975. Topographically generated internal waves in the open ocean. *Journal of Geophysical Research* 80:320–327, <https://doi.org/10.1029/JC080i003p00320>.
- Bogucki, D., T. Dickey, and L.G. Redekopp. 1997. Sediment resuspension and mixing by resonantly generated internal solitary waves. *Journal of Physical Oceanography* 27:1181–1196, [https://doi.org/10.1175/1520-0485\(1997\)027<1181:SRAMBR>2.0.CO;2](https://doi.org/10.1175/1520-0485(1997)027<1181:SRAMBR>2.0.CO;2).
- Bogucki, D., and C. Garrett. 1993. A simple model for the shear induced decay of an internal solitary wave. *Journal of Physical Oceanography* 23:1–10, [https://doi.org/10.1175/1520-0485\(1993\)023<1767:ASMFTS>2.0.CO;2](https://doi.org/10.1175/1520-0485(1993)023<1767:ASMFTS>2.0.CO;2).
- Buijsman, M.C., J.K. Ansong, B.K. Arbic, J.G. Richman, J.F. Shriver, P.G. Timko, A.J. Wallcraft, C.B. Whalen, and Z.X. Zhao. 2016. Impact of parameterized internal wave drag on the semidiurnal energy balance in a global ocean circulation model. *Journal of Physical Oceanography* 46(5):1,399–1,419, <https://doi.org/10.1175/JPO-D-15-0074.1>.
- Chen, Z., Y. Nie, J. Xie, J. Xu, Y. He, and S. Cai. 2017. Generation of internal solitary waves over a large sill: From Knight Inlet to Luzon Strait. *Journal of Geophysical Research* 122:1,555–1,573, <https://doi.org/10.1002/2016JC012206>.
- Combes, V., and R.P. Matano. 2014. Trends in the Brazil/Malvinas Confluence region. *Geophysical Research Letters* 41:8,971–8,977, <https://doi.org/10.1002/2014GL062523>.
- da Silva, J.C.B., M.C. Buijsman, and J.M. Magalhães. 2015. Internal waves on the upstream side of a large sill of the Mascarene Ridge: A comprehensive view of their generation mechanisms and evolution. *Deep Sea Research Part I* 99:87–104, <https://doi.org/10.1016/j.dsr.2015.01.002>.
- da Silva, J.C.B., S.A. Ermakov, and I.S. Robinson. 2000. Role of surface films in ERS-SAR signatures of internal waves on the shelf: Part 3. Mode transitions. *Journal of Geophysical Research* 105:24,089–24,104, <https://doi.org/10.1029/2000JC900053>.
- da Silva, J.C.B., and K.R. Helfrich. 2008. Synthetic Aperture Radar observations of resonantly generated internal solitary waves at Race Point Channel (Cape Cod). *Journal of Geophysical Research* 113, C11016, <https://doi.org/10.1029/2008JC005004>.
- da Silva, J.C.B., A.L. New, and J.M. Magalhães. 2009. Internal solitary waves in the Mozambique Channel: Observations and interpretation. *Journal of Geophysical Research* 114, C05001, <https://doi.org/10.1029/2008JC005125>.
- Egbert, G.D., and S.Y. Erofeeva. 2002. Efficient inverse modeling of barotropic ocean tides. *Journal of Oceanic and Atmospheric Technology* 19:183–204, [https://doi.org/10.1175/1520-0426\(2002\)019<0183:EIMOBO>2.0.CO;2](https://doi.org/10.1175/1520-0426(2002)019<0183:EIMOBO>2.0.CO;2).
- Etcheverry, L.A.R., M. Saraceno, A.R. Piola, and P.T. Strub. 2016. Sea level anomaly on the Patagonian continental shelf: Trends, annual patterns and geostrophic flows. *Journal of Geophysical Research* 121:2,733–2,754, <https://doi.org/10.1002/2015jc011265>.
- Farmer, D.M., and L. Armi. 1999. The generation and trapping of internal solitary waves over topography. *Science* 283:188–190, <https://doi.org/10.1126/science.283.5399.188>.
- Jackson, C.R. 2004. *An Atlas of Internal Solitary-like Waves and their Properties*, 2nd ed. Global Ocean Associates, Alexandria, VA, 560 pp., <http://www.internalwaveatlas.com>.
- Jackson, C.R. 2007. Internal wave detection using the Moderate Resolution Imaging Spectroradiometer (MODIS). *Journal of Geophysical Research* 112, C11012, <https://doi.org/10.1029/2007JC004220>.
- Jackson, C.R., and W. Alpers. 2010. The role of the critical angle in brightness reversals on sunglint images of the sea surface. *Journal of Geophysical Research* 115, C09019, <https://doi.org/10.1029/2009JC006037>.
- Jackson, C.R., J.C.B. da Silva, and G. Jeans. 2012. The generation of nonlinear internal waves. *Oceanography* 25(2):108–123, <https://doi.org/10.5670/oceanog.2012.46>.
- Kodaira, T., T. Waseda, and Y. Miyazawa. 2014. Nonlinear internal waves generated and trapped upstream of islands in the Kuroshio. *Geophysical Research Letters* 41:5,091–5,098, <https://doi.org/10.1002/2014GL060113>.
- Lentini, C.A.D., J.M. Magalhães, J.C.B. da Silva, and J.A. Lorenzetti. 2016. Transcritical flow and generation of internal solitary waves off the Amazon River: Synthetic aperture radar observations and interpretation. *Oceanography* 29(4):187–195, <https://doi.org/10.5670/oceanog.2016.88>.
- Magalhães, J.M., and J.C.B. da Silva. 2012. SAR observations of internal solitary waves generated at the Estremadura Promontory off the west Iberian coast. *Deep-Sea Research Part I* 69:12–24, <https://doi.org/10.1016/j.dsr.2012.06.002>.
- Melville, W.K., and K.R. Helfrich. 1987. Transcritical two-layer flow over topography. *Journal of Fluid Mechanics* 178:31–52, <https://doi.org/10.1017/S0022112087001101>.
- Mugetti, A., C. Brieve, S. Giangiobbe, E. Gallicchio, F. Pacheco, A. Pagani, A. Calcagno, S. González, O. Natale, M. Faure, and others. 2004. *Patagonian Shelf, GIWA Regional Assessment* 38. UNEP, University of Kalmar, Kalmar, Sweden, 164 pp. plus appendixes, <http://wedocs.unep.org/handle/20.500.11822/8792>.
- Nikurashin, M., and R. Ferrari. 2010. Radiation and dissipation of internal waves generated by geostrophic flows impinging on small-scale topography: Theory. *Journal of Physical Oceanography* 40:1,055–1,074, <https://doi.org/10.1175/2009JPO4199.1>.
- Nikurashin, M., and R. Ferrari. 2011. Global energy conversion rate from geostrophic flows into internal lee waves in the deep ocean. *Geophysical Research Letters* 38, L08610, <https://doi.org/10.1029/2011GL046576>.
- Piola, A.R., B.C. Franco, E.D. Palma, and M. Saraceno. 2013. Multiple jets in the Malvinas Current. *Journal of Geophysical Research* 118:2,107–2,117, <https://doi.org/10.1002/jgrc.20170>.
- Redekopp, L.G., and Z. You. 1995. Passage through resonance for the forced Korteweg de Vries equation. *Physical Review Letters* 74(26):5,158–5,161, <https://doi.org/10.1103/physrevlett.74.5158>.
- Smith, W.H.F., and D.T. Sandwell. 1997. Global sea-floor topography from satellite altimetry and ship depth soundings. *Science* 277:1,957–1,962, <https://doi.org/10.1126/science.277.5334.1956>.
- Smyth, W.D., J.N. Moum, and J.D. Nash. 2011. Narrowband oscillations in the upper equatorial ocean: Part II. Properties of shear instabilities. *Journal of Physical Oceanography* 41(3):412–428, <https://doi.org/10.1175/2010JPO4451.1>.
- Thompson, D.R., and R.F. Gasparovic. 1986. Intensity modulation in SAR images of internal waves. *Nature* 320:345–348, <https://doi.org/10.1038/320345a0>.
- Trossman, D.S., B.K. Arbic, J.G. Richman, S.T. Garner, S.R. Jayne, and A.J. Wallcraft. 2016. Impact of topographic internal lee wave drag on an eddying global ocean model. *Ocean Modelling* 97:109–128, <https://doi.org/10.1016/j.ocemod.2015.10.013>.

## ACKNOWLEDGMENTS

The authors would like to acknowledge ESA project AOPT-2423 and DLR projects OCE3154 and OCE2254 for providing the SAR images. J. da Silva and J.M. Magalhães are grateful to Brazilian CNPq project 313603/2013-8. J.M. Magalhães is also grateful for an FCT research grant (SFRH/BPD/84420/2012). Contributions from anonymous reviewers are acknowledged for greatly improving the original version of the paper.

## AUTHORS

**Jorge M. Magalhães** ([jmagalhaes@fc.ul.pt](mailto:jmagalhaes@fc.ul.pt)) is Postdoctoral Researcher and **José C.B. da Silva** is Associate Professor, Department of Geosciences, Environment, and Spatial Planning, and Interdisciplinary Centre of Marine and Environmental Research, University of Porto, Porto, Portugal.

## ARTICLE CITATION

Magalhães, J.M., and J.C.B. da Silva. 2017. Internal waves along the Malvinas Current: Evidence of transcritical generation in satellite imagery. *Oceanography* 30(3):110–119, <https://doi.org/10.5670/oceanog.2017.319>.